

RESEARCH ARTICLE

Manganese-porphyrin-enhanced MRI for the detection of cancer cells: A quantitative *in vitro* investigation with multiple clinical subtypes of breast cancer

Mosa Alhamami^{1,2,3}, Weiran Cheng^{4,5}, Yuanyuan Lyu^{5,6}, Christine Allen^{1,2,7}, Xiaohan Zhang^{4,5,8}, Hai-Ling Margaret Cheng^{1,2,3,9,10*}

1 Department of Pharmaceutical Sciences, Leslie Dan Faculty of Pharmacy, University of Toronto, Toronto, Ontario, Canada, **2** Institute of Biomaterials and Biomedical Engineering, University of Toronto, Toronto, Ontario, Canada, **3** Translational Medicine, Hospital for Sick Children Research Institute, Toronto, Ontario, Canada, **4** Department of Chemistry, University of Toronto, Toronto, Ontario, Canada, **5** Department of Physical and Environmental Sciences, University of Toronto Scarborough, Toronto, Ontario, Canada, **6** School of Medicine, Zhejiang University City College, Hangzhou, Zhejiang, P. R. China, **7** Spatio-Temporal Targeting and Amplification of Radiation Response (STTARR) Innovation Centre, Radiation Medicine Program, Princess Margaret Cancer Centre, University Health Network, Toronto, Ontario, Canada, **8** Department of Biological Sciences, University of Toronto Scarborough, Toronto, Ontario, Canada, **9** The Edward S. Rogers Sr. Department of Electrical and Computer Engineering, University of Toronto, Toronto, Ontario, Canada, **10** Translational Biology and Engineering Program, Ted Rogers Centre for Heart Research, Toronto, Ontario, Canada

* hailing.cheng@utoronto.ca



OPEN ACCESS

Citation: Alhamami M, Cheng W, Lyu Y, Allen C, Zhang X-a, Cheng H-LM (2018) Manganese-porphyrin-enhanced MRI for the detection of cancer cells: A quantitative *in vitro* investigation with multiple clinical subtypes of breast cancer. PLoS ONE 13(5): e0196998. <https://doi.org/10.1371/journal.pone.0196998>

Editor: Bing Xu, Brandeis University, UNITED STATES

Received: January 26, 2018

Accepted: April 24, 2018

Published: May 24, 2018

Copyright: © 2018 Alhamami et al. This is an open access article distributed under the terms of the [Creative Commons Attribution License](https://creativecommons.org/licenses/by/4.0/), which permits unrestricted use, distribution, and reproduction in any medium, provided the original author and source are credited.

Data Availability Statement: All data files are available from the TSpace Repository database (URL: <http://hdl.handle.net/1807/87713>).

Funding: Funded by Heart & Stroke Foundation of Canada (#000223 to HLMC) <http://www.heartandstroke.ca/>. Natural Sciences and Engineering Research Council of Canada (#355795 to HLMC) http://www.nserc-crsng.gc.ca/index_eng.asp. SickKids Foundation (to HLMC). NSERC Alexander Graham Bell Canada Graduate

Abstract

Magnetic resonance imaging (MRI) contrast agents (CAs) are chemical compounds that can enhance image contrast on T₁- or T₂- weighted MR image. We have previously demonstrated the potential of MnCl₂, a manganese-based CA, in cellular imaging of breast cancer using T₁-weighted MRI. In this work, we examined the potential of another class of manganese-based CAs, manganese porphyrins (MnPs), for sensitive cellular detection of multiple clinical subtypes of breast cancer using quantitative MRI. Using a clinical 3.0-T MRI scanner, the relaxivities of two MnPs, MnTPPS₄ and MnTPPS₃NH₂, and conventional Gd-DTPA (control) were measured in ultrapure water and their T₁ contrast enhancement patterns were characterized in multiple clinical subtypes of breast cancer. The toxicity of the three CAs was evaluated *in vitro*. Compared to Gd-DTPA, both MnTPPS₃NH₂ and MnTPPS₄ enabled a more sensitive multi-subtype detection of four breast cell lines at doses that posed no cytotoxic effects, with MnTPPS₃NH₂ producing the greatest positive enhancement. The superior T₁ enhancement capabilities of MnPs over Gd-DTPA are statistically significant and are likely due to their greater cellular uptake and relaxivities. The results demonstrate that multiple clinical subtypes of breast cancer can be imaged on a 3.0-T MRI scanner using MnPs as T₁ cellular CAs.

Scholarships - Doctoral (to MA), Ontario Graduate Scholarship (to MA), National Science Foundation of China (#51303155 to YL). The funders had no role in study design, data collection and analysis, decision to publish, or preparation of the manuscript.

Competing interests: The authors have declared that no competing interests exist.

Introduction

Clinically, gadolinium–diethylenetriamine pentaacetic acid (Gd-DTPA)-enhanced MRI is used, in conjunction with X-ray mammography, for screening women who are at high risk (lifetime risk ≥ 20 –25%) of developing breast cancer [1]. Gd-DTPA-enhanced MRI is also relied upon routinely to delineate vasculature and tumor extent once suspicious findings are initially identified with X-ray mammography. However, as a T_1 contrast agent (CA), Gd-DTPA is associated with a number of critical limitations. These include toxicity due to potential dissociation of Gd from the DTPA chelator [2], relatively low relaxivity [3], and rapid distribution into and wash out from malignant sites. In fact, due to the low tumor retention and temporally diminished contrast effect of Gd-DTPA, its post-contrast imaging window is often limited to few minutes [1,4].

Engineering CAs that can be taken up and retained by cells could enable sensitive detection and visualization of labelled cells over a relatively long (e.g. ≥ 20 hrs) imaging window, thereby providing information on physiological processes at the cellular level. Cellular CAs can either shorten the longitudinal relaxation time T_1 (positive enhancement) or the transverse relaxation time T_2 (negative enhancement). T_1 -shortening cellular CAs increase signal intensity (i.e. produce image brightening) with T_1 -weighted MRI parameters, while T_2 -shortening cellular CAs decrease signal intensity (i.e. produce image darkening) with T_2 - or T_2^* -weighted MRI parameters [5]. However, a fundamental drawback of T_2 -shortening CAs in MRI is the lack of specificity; distinction of T_2 CA-labelled cells is difficult due to the intrinsic low signal intensity or negative contrast that may arise from some background, CA-free biologic tissues. Therefore, it is highly desirable to design and evaluate T_1 CAs that can be efficiently internalized by cells. By virtue of their cellular uptake and retention within the tumor site, these CAs can provide sensitive and persistent identification of labelled cells, improving tumor imaging window even in less vascularized masses. Additionally, cellular CAs, unlike Gd-DTPA, can allow sensitive detection of cancer cells directly at an early stage, when vasculature has not been fully formed at tumor site. In fact, recent work using $MnCl_2$ as a T_1 cellular CA demonstrated the potential of MRI as a cellular imaging modality that is capable of directly detecting breast cancer cells *in vitro* [6] as well as characterizing the metastatic potential of early small (≤ 5 mm³) breast tumors in mice [7]. Moreover, the same research group demonstrated that larger, more advanced breast tumors that did not enhance on Gd-DTPA underwent substantial enhancement with $MnCl_2$ [8].

Manganese porphyrin (MnP) is another class of Mn-based CAs that can produce positive enhancement on T_1 -weighted MRI [9–11] with multiple routes of administration, including intravenous injections [12]. MnPs offer several advantages over conventional Gd-DTPA. First, because the porphyrin ring binds Mn^{3+} with high stability, the likelihood of ion release in MnPs is very low. In fact, the most extensively investigated MnP, manganese (III) tetraphenyl porphyrin sulfonate ($MnTPPS_4$), exhibited no demetallation *in vitro* in human plasma for up to 9 days [13] and only about 1% degree of demetallation *in vivo* in liver and kidney up to 4 days post administration [14]. Additionally, MnPs have higher relaxivities than Gd-DTPA [12,15]; specifically, $MnTPPS_4$ has recently been shown to have a lower minimum detectable concentration and a greater sensitivity than Gd-DTPA in phosphate buffered saline [16]. Therefore, MnPs can achieve a positive contrast enhancement similar to Gd-DTPA but at lower doses, which reduces their systemic toxicity. Previous studies have specifically explored the potential of $MnTPPS_4$ as a tumor-seeking agent. In addition to tumor characteristics (high capillary permeability, poor lymphatic drainage, and large interstitial fluid space), Fiel *et al.* attributed the localization of $MnTPPS_4$ in L1210 solid tumors grown in mice to the size of the planar porphyrin ring, favoring its retention and aggregation in tumors [14]. Also, Fiel *et al.*

demonstrated cellular uptake of MnTPPS₄ in L1210 tumors *in vivo* and noted that by increasing the hydrophobicity of porphyrins, they would be transported across plasma membranes more readily [14]. Shortly thereafter, Place *et al.* reported the greater uptake of MnTPPS₄ in MCF-7 breast cancer cells (× 175 after 24 hrs) compared to a normal breast cell line (Hs578Bst) *in vitro* [17]. The temporally regulated tumor retention efficacy of MnTPPS₄ was also demonstrated *in vivo* in several tumor models [12,18,19]. However, there has been no experimental evidence pertaining to the capability of MnTPPS₄-enhanced MRI in detecting multiple clinical subtypes of breast cancer.

The purpose of this work is to determine whether MnTPPS₄ is capable of directly detecting multiple clinical subtypes of breast cancer cells (Table 1) compared to Gd-DTPA, used previously in cell labelling studies [20–22]. This work also aims at determining whether an amino MnP, known as MnTPPS₃NH₂ (see S1 Fig), can provide more sensitive cellular detection of breast cancer cells than MnTPPS₄, thereby lowering the dose needed to achieve positive enhancement on T₁-weighted MR image.

Zhang *et al.* previously synthesized MnTPPS₃NH₂ and conjugated it to dextran [23]. Compared to Gd-DTPA, MnTPPS₃NH₂-dextran conjugate enabled a greater and more prolonged signal enhancement on T₁-weighted MRI, possibly due to the binding of dextran to cell membranes which facilitates the targeting of MnTPPS₃NH₂ to tumor cells [23]. However, to the best of our knowledge, no previous work has investigated the potential of the unconjugated MnTPPS₃NH₂ as a T₁ CA for sensitive detection of multiple clinical subtypes of breast cancer cells using quantitative MRI.

It is hypothesized that MnP-enhanced MRI is capable of enabling a more substantial enhancement of various subtypes of breast cancer cells compared to conventional Gd-DTPA-enhanced MRI. It is further hypothesized that MnTPPS₃NH₂ is a more effective T₁ CA than MnTPPS₄ for multi-subtype detection of breast cancers using quantitative MRI due to its higher hydrophobicity and cellular uptake.

Materials and methods

Contrast agent solutions preparation and sterilization

To make the first stock solution of the CAs, autoclaved, ultrapure water (MilliQ Purification System, Millipore, Darmstadt, Germany) was added to MnTPPS₄ (5,10,15,20-Tetrakis(4-sulfonatophenyl)-21H,23H-porphine manganese(III) chloride, Sigma-Aldrich Canada Co., Oakville ON, Product# 441813) and MnTPPS₃NH₂ (synthesized in our laboratory). The CA solutions were filtered using a 33-mm-diameter sterile Millex-GP syringe filter unit with a 0.22-µm pore size hydrophilic polyethersulfone membrane (SLGP033RS, Millipore, Darmstadt, Germany). The first stock solutions were sono-bathed in an ultrasonic cleaner (VWR symphony, VWR International, Mississauga, Canada) for 30 minutes at about 65 °C. To further sterilize and solubilize the stock solutions, they were placed at a hotplate, preheated at

Table 1. The clinical subtypes and molecular classification of breast cancer cell lines used in this study (adapted from references [24,25]).

Cell line	Classification / subtype	Tumorigenicity	Receptor expression
MDA-MB-231	Claudin low[24]; basal-like[25]	Tumorigenic	ER ⁻ , PR ⁻ , HER2 ⁻
MCF-7	Luminal A[24,25]	Tumorigenic	ER ⁺ , PR ^{+/-} , HER2 ⁻
ZR-75-1	Luminal B[24]; luminal A[25]	Tumorigenic	ER ⁺ , PR ^{+/-} , HER2 ^{+/-}
MCF-10A	Basal-like[25]	Non-tumorigenic	ER ⁻ , PR ⁻ , HER2 ⁻

ER, estrogen receptor; PR, progesterone receptor; HER2, human epidermal growth factor receptor 2.

<https://doi.org/10.1371/journal.pone.0196998.t001>

100–200 °C, for approximately 5–7 minutes. Serial dilutions (1000X) were made inside a bio-safety cabinet in order to decrease the concentrations of the sterilized first stock solutions of the CAs to detectable levels on a UV-visible spectrophotometer. The concentrations of the diluted solutions were then determined by measuring absorbance using a UV-visible spectrophotometer. Knowing the dilution factors, the concentrations of the first stock solutions of the CAs were found.

Relaxivity measurements

Stock solutions of the three CAs used in this study, MnTPPS₄, MnTPPS₃NH₂ and Gd-DTPA (Magnevist, Bayer HealthCare LLC, Whippany, NJ), were prepared in ultrapure MilliQ water at concentrations 0, 0.05, 0.1 and 0.2 mM per metal ion. The solutions were transferred to 115 × 5 mm wintrobe sedimentation tubes (Kimble Chase, Vineland, NJ). A total of 30 sedimentation tubes were loaded with CA solutions at the aforementioned concentrations (three tubes for each CA dissolved at a given concentration). The sedimentation tubes were then placed in an upright position in an ultem resin (McMaster-Carr, Chicago, IL) holder and transferred to the MRI suite. The ultem resin holder, with the sedimentation tubes containing CA solutions, was placed within a 32-channel receive/transmit head coil. MRI was performed on a 3.0-T MRI scanner (Achieva 3.0 T TX, Philips Medical Systems, Best, the Netherlands). Longitudinal and transverse relaxivities, r_1 and r_2 , were determined by measuring T_1 and T_2 relaxation times for each CA solution at the aforementioned concentrations and calculating the slope of the linear regression model fitted on a $1/T_1$ (longitudinal relaxation rate) or $1/T_2$ (transverse relaxation rate) versus CA concentration, [CA]. CA-induced changes in longitudinal and transverse relaxation rates are given by the following mathematical expressions, where $\frac{1}{T_1}$ and $\frac{1}{T_2}$ are intrinsic relaxation rates without CA:

$$\frac{1}{T_1} = \frac{1}{T_1'} + r_1 \times [CA] \tag{1}$$

$$\frac{1}{T_2} = \frac{1}{T_2'} + r_2 \times [CA] \tag{2}$$

To measure T_1 relaxation times, a two-dimensional (2D) inversion-recovery turbo spin-echo (IR-TSE) sequence was utilized with the following parameters: inversion times (TI) = [50, 100, 250, 500, 750, 1000, 1250, 1500, 2000, 2500] ms, repetition time (TR) = 3000 ms, echo time (TE) = 18.5 ms, slice thickness = 7 mm, field-of-view (FOV) = 60 × 60 mm, in-plane resolution = 0.5 × 0.5 mm, and TSE factor = 4. T_2 relaxation times were measured using a multi-spin-multi-echo (MSME) spin-echo sequence with the following parameters: TR = 2000 ms, 32 echoes with TE = [7.6, 15.3, 22.9 . . . 244.0], slice thickness = 7 mm, FOV = 60 × 60 mm, and in-plane resolution = 0.5 × 0.5 mm.

Cell culture

The human breast cancer cell lines MDA-MB-231, MCF-7, and ZR-75-1 as well as a non-tumorigenic breast epithelial cell line, MCF-10A, were obtained from ATCC (American Tissue Culture Collection, Manassas, VA) and used in this study. The cells were maintained at 37 °C with 5% CO₂ in their recommended culture media: MDA-MB-231 in high glucose-containing Dulbecco's Modification of Eagle's Medium (DMEM), 1X (cat. # 319-005-CL, Wisent Inc., Saint-Jean-Baptiste, QC, Canada); MCF-7 in Eagle's Minimum Essential Medium (EMEM) (ATCC cat. # 30-2003) supplemented with 0.01 mg/mL bovine insulin (Sigma-Aldrich cat. #

I0516); ZR-75-1 in RPMI-1640 (ATCC cat. # 30–2001); MCF-10A in Mammary Epithelial Base Medium (MEBM) supplemented with additives (Lonza MEGM kit cat. # CC-3150). These additives, which are provided with the kit, include 2 mL bovine pituitary extract (BPE), 0.5 mL human epidermal growth factor (hEGF), 0.5 mL hydrocortisone, and 0.5 mL insulin. In addition, 100 ng/mL cholera toxin (Sigma-Aldrich cat. # C8052) was added to make the complete growth medium for MCF-10A, as per ATCC recommendations. The aforementioned four growth media were supplemented with 10% (v/v) fetal bovine serum (FBS) (ATCC cat. # 30–2020).

The cultures were initiated by thawing an ATCC cryo-vial that had been stored in liquid nitrogen (vapor phase) and plating the cells in a T-25 flask (Sarstedt Inc., Montreal, QC, Canada). When the flask was 80–90% confluent, the cells were passaged to T-175 flasks after washing them once with Dulbecco's Phosphate Buffered Saline (DPBS, without calcium and magnesium), 1X (ATCC cat. # 30–2200) and adding trypsin-EDTA solution, 1X (0.25% trypsin / 0.53 mM ethylenediaminetetraacetic acid) without calcium and magnesium (ATCC cat. # 30–2101) for 4–5 minutes (MDA-MB-231, MCF-7, and ZR-75-1) or 0.05% trypsin / 0.02% EDTA (ATCC cat. # PCS-999-003) for at least 20 minutes (MCF-10A). The trypsin-EDTA solution was deactivated by adding a serum-supplemented medium. Prior to plating in new flasks, the cells were centrifuged at 125 *xg* at room temperature for 5 minutes. The supernatant containing the deactivated trypsin-EDTA and medium mixture was aspirated and replaced with fresh, serum-supplemented medium.

Cell labelling with CAs and preparation for MRI

Labelling MDA-MB-231 cells at varying CA concentrations: CA direct exposure and retention experiments. The initial fundamental experiments evaluated the three CAs with an aggressive, triple-negative breast cancer cell line, MDA-MB-231, at varying concentrations and incubation conditions (CA direct exposure and cellular retention). Solutions of the CAs were added to MDA-MB-231 complete growth medium (DMEM + 10% FBS) at 0.05, 0.1 and 0.2 mM. The CA-containing complete growth media were then shaken to ensure uniform distribution and were administered to 9 T-175 flasks (3 for each CA, covering the three concentrations) of MDA-MB-231 cells growing in the exponential growth phase. The 9 CA-containing T-175 flasks and another CA-free T-175 flask (control), which had also undergone a medium change at the time of CA administration, were incubated for up to 23 hours at 37 °C in 5% CO₂. Subsequently, the cells were rinsed once with DPBS, trypsinized with trypsin-EDTA solution for about 4 minutes, and centrifuged at 125 *xg* at room temperature for 5 minutes. Because the trypsin-EDTA solution was deactivated with the original CA-containing medium in each one of the 9 T-175 flasks, the cells were rinsed again with DPBS immediately following the aspiration of the supernatant. This step was followed by another centrifugation, also at 125g at room temperature for 5 minutes, the removal of the DPBS supernatant, and the addition of a fresh, serum-free growth medium (i.e. only DMEM) to each centrifuge tube. The cell suspensions from the 10 T-175 flasks were collected in ten separate 50-mL conical centrifuge tubes and were subsequently transferred to 115 × 5 mm Wintrobe sedimentation tubes. Each one of the 10 sedimentation tubes was placed in a larger 15-mL centrifuge tube and spun, for the last time prior to MRI, at 440 *xg* at room temperature for 15 minutes to create cell pellets for MRI. The opening of each sedimentation tube was secured firmly with a tape.

The aforementioned procedures were performed on two sets of 10 T-175 flasks: the CA direct-exposure set and the CA cellular retention set. In the CA direct-exposure set, the cells were incubated with the CAs for up to 23 hours at 37 °C in 5% CO₂ and cell pellets were prepared for MRI immediately following the removal of the CA-containing media as described

above. In the CA cellular retention set, after 23–24 hours of incubation with the CAs at 37 °C in 5% CO₂, the cells were rinsed twice with DPBS following the removal of the CA-containing media from the T-175 flasks, supplemented with fresh, CA-free complete growth medium (DMEM + 10% FBS), and allowed to grow in CA-free medium for an additional 24–27 hours at 37 °C in 5% CO₂ to examine the differential capability of the three CAs in being retained intracellularly at varying incubation concentrations. At the end of the incubation period, cell pellets for the CA cellular retention set were prepared for MRI as previously described.

CA labelling of multiple clinical subtypes of breast cancer. In order to evaluate the capability of the proposed quantitative cellular MRI approach for sensitive detection of multiple clinical subtypes of breast cancer, the four breast cell lines (Table 1) were labelled with the three CAs at 0.2 mM following the aforementioned CA direct-exposure labelling protocol at approximately a 24-hr labelling interval. A control (unlabelled) cell pellet was also prepared for each cell line.

Cytotoxicity assessment of CA-labelled breast cell lines

Cell viability of CA-labelled breast cell lines was assessed by trypan blue exclusion method with an automated cell viability analyzer (Vi-CELL XR cell viability analyzer, Beckman Coulter Inc., Mississauga, Canada) to determine whether labelling with any one of the three CAs had cytotoxic effects on the four breast cell lines. Briefly, cells were plated in 96-well assay plates (Corning Costar, Corning, NY) at a cell density of about $15\text{--}20 \times 10^3$ cells/well, thoroughly suspended in a medium volume of 150 μL , using an X-stream repeater pipette (Eppendorf, Mississauga, Canada) such that there are five replicates for the cells that would later be labelled with Gd-DTPA, MnTPPS₄, or MnTPPS₃NH₂. Another two 5-well replicates were plated around the 15 CA wells for the unlabelled (control) cells (see S2 Fig). After seeding a total of 25 wells in each 96-well plate, the cells were incubated at 37 °C in 5% CO₂ to allow recovery from trypsinization and adherence to the culture plates. To avoid evaporation and edge effects, the 25 experimental wells in each 96-well plate for each cell line were placed in the middle of the plate, whereas all of the other remaining no-cell wells were filled with complete growth media at a volume slightly higher than the experimental wells (170 μL). After the two-day incubation period, cells were labelled with CAs at 0.2 mM for 24–27 hours at 37 °C in 5% CO₂. At the end of the labelling interval, cells from each well were washed with DPBS, trypsinized and harvested, as previously described, in 2-mL microtubes. The viability was then assessed using Vi-CELL viability analyzer for each well. Cell morphology was observed and mean diameter was measured using the analyzer.

MRI of CA-labelled breast cancer cell lines

After preparing CA-labelled cell pellets, the sedimentation tubes were placed in an upright position in an ultem resin holder and transferred in a styrofoam ice box to the MRI suite. The ultem resin holder, with the sedimentation tubes containing cell pellets, was placed within a 32-channel receive/transmit head coil and MRI was performed on the 3.0-T MRI scanner.

Quantitative T₁ and T₂ relaxation times were measured using the same IR-TSE and MSME sequences utilized previously in the relaxivity measurements. However, due to the shallow depth of some cell pellets, the slice thickness had to be adjusted to 2.5 mm and 2.0 mm during the scans. High-resolution T₁-weighted images were also acquired using a 2D spin-echo sequence with the following parameters: TR = 167 ms, TE = 14.2 ms, FOV = 60 × 60 mm, flip angle = 90°, number of signal averages = 8, in-plane resolution = 0.5 × 0.5 mm, and slice thickness = 2.5 mm (CA direct-exposure scan with MDA-MB-231 and multi-cell line scan) and 2.0 mm (CA cellular retention scan with MDA-MB-231).

Quantitative MRI data analysis

Quantitative analysis of the MRI data was performed using in-house software developed in MATLAB (R2014a, version 8.3, MathWorks, Natick, MA). To calculate T_1 and T_2 relaxation times, regions of interest (ROIs) were outlined within each cell pellet- or CA solution-containing sedimentation tube in the MR images. Calculation of the relaxation times was performed on a pixel-by-pixel basis in each pellet/tube. To compute a quantitative map of T_1 relaxation times, T_1 was calculated at each pixel within an ROI by fitting the signal intensity versus TI at that pixel to the following function:

$$A \times \left| 1 - 2\exp\left(-\frac{TI}{T_1}\right) + \exp\left(-\frac{TR}{T_1}\right) \right| \quad (3)$$

where A and T_1 are free parameters.

A quantitative map of T_2 relaxation times was computed by calculating T_2 at each pixel within an ROI through fitting the signal intensity versus TE at that pixel to a mono-exponential decay function added to a constant offset to account for noise. The T_1 and T_2 relaxation times for each ROI within the breast cancer cell pellets represent mean values \pm standard deviations from all the pixels within that ROI in the quantitative maps of T_1 and T_2 , respectively. The longitudinal and transverse relaxivities, r_1 and r_2 , were determined by linear regression analysis on the change in the inverse of relaxation times ($1/T_1$ and $1/T_2$) versus CA concentration.

Statistical analysis

To investigate the significance in the differences of means of relaxation times, a Student's t-test was performed at the 95% confidence level ($P = 0.05$). The number of pixels in each cell pellet's ROI was used as the sample size (n) in calculating the 95% confidence intervals for two-sample comparisons of relaxation times using in-house software developed in MATLAB.

Results

Longitudinal and transverse relaxivity measurements

[Fig 1A and 1B](#) show the $1/T_1$ (longitudinal relaxation rate) and $1/T_2$ (transverse relaxation rate) as a function of CA concentration for MnTPPS₃NH₂, MnTPPS₄ and Gd-DTPA in MilliQ water at 3.0 T and room temperature. Shown also are the fitted linear regression lines along with the corresponding R^2 . Longitudinal and transverse relaxivity constants, r_1 and r_2 , of the three CAs were calculated from the linear regression slopes of graphs (a) and (b), respectively, and are summarized in [Table 2](#). A more than 2.5-fold and 2-fold increase in longitudinal relaxivity was attained for MnTPPS₃NH₂ ($r_1 = 9.33 \text{ mM}^{-1} \text{ s}^{-1}$) and MnTPPS₄ ($r_1 = 7.99 \text{ mM}^{-1} \text{ s}^{-1}$), respectively, over Gd-DTPA ($r_1 = 3.58 \text{ mM}^{-1} \text{ s}^{-1}$). However, the r_2/r_1 ratios for the three CAs are close to unity at relatively low CA concentrations.

Quantitative MRI of MDA-MB-231 cells labelled with varying CA concentrations

CA direct exposure results. [Fig 2A](#) shows a quantitative map of T_1 relaxation times of MDA-MB-231 cell pellets following direct exposure to CAs. The largest decrease in T_1 of the MnTPPS₃NH₂-labelled cell pellet at 0.2 mM (53.3%) corresponds to the greatest positive signal enhancement on T_1 -weighted MRI compared to the unlabelled cell pellet. MnTPPS₄ provided a 36.6% reduction in T_1 , whereas Gd-DTPA offered only a 16.5% decrease in T_1 at 0.2 mM,

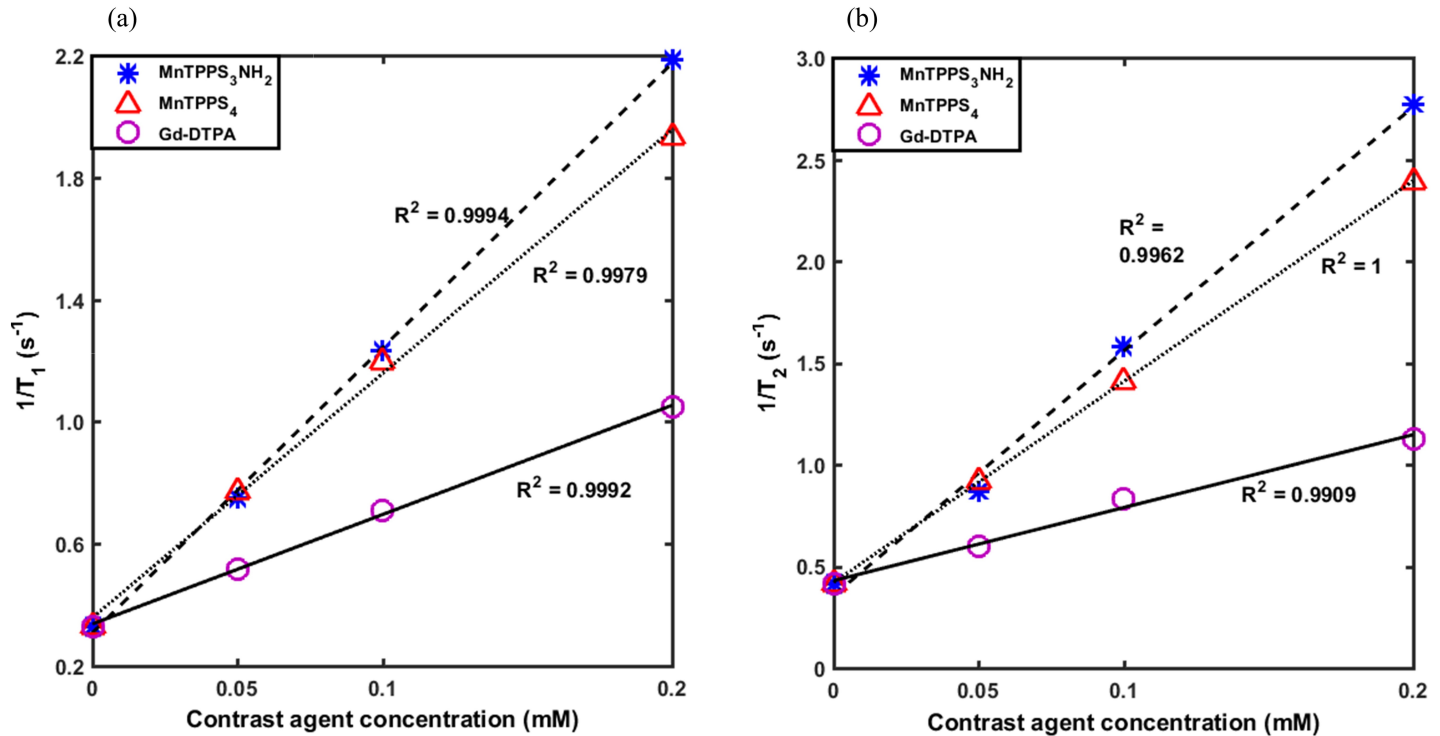


Fig 1. Relaxivity measurements. The measured (a) $1/T_1$ and (b) $1/T_2$ values as a function of CA concentration for the three CAs in MilliQ water at 3.0 T and room temperature. Shown also are the fitted linear regression lines and the corresponding R^2 values.

<https://doi.org/10.1371/journal.pone.0196998.g001>

both relative to unlabelled cell pellet. The aforementioned differences are statistically significant at 95% confidence level.

Fig 2B and 2C show the averaged T_1 and T_2 relaxation times of the aforementioned CA labelled cell pellets. The values represent mean \pm standard deviation from all the pixels within each ROI in the quantitative maps of T_1 , Fig 2A, and T_2 relaxation times. For each CA, the difference among the T_1 times at 0, 0.05, 0.1, and 0.2 mM is statistically significant ($P < 0.05$). At each CA concentration, the difference among the CAs is also statistically significant ($P < 0.05$). In fact, between 0.05–0.2 mM, MnTPPS₃NH₂ produced a 10.6% to 26.4% reduction in T_1 compared to MnTPPS₄, which enabled a further 13.2% to 24.1% reduction in T_1 over Gd-DTPA. The greatest reduction in T_1 times among the CAs is measured at 0.2 mM. On the other hand, the induced CA dose-dependent changes on T_2 times of MDA-MB-231 cells are primarily insignificant at 95% confidence level for the three CAs.

CA cellular retention results. A quantitative map of T_1 relaxation times of the CA cellular retention cell pellets is shown in Fig 3A. Fig 3B shows the averaged T_1 relaxation times for the aforementioned cell pellets. The values represent mean \pm standard deviation from all the pixels

Table 2. Longitudinal and transverse relaxivity constants (r_1 and r_2) measured at 3.0 T at room temperature.

Contrast agent	r_1	r_2
MnTPPS ₃ NH ₂	9.33	12.00
MnTPPS ₄	7.99	9.87
Gd-DTPA	3.58	3.58

Units for r_1 and r_2 are in mM⁻¹ s⁻¹.

<https://doi.org/10.1371/journal.pone.0196998.t002>

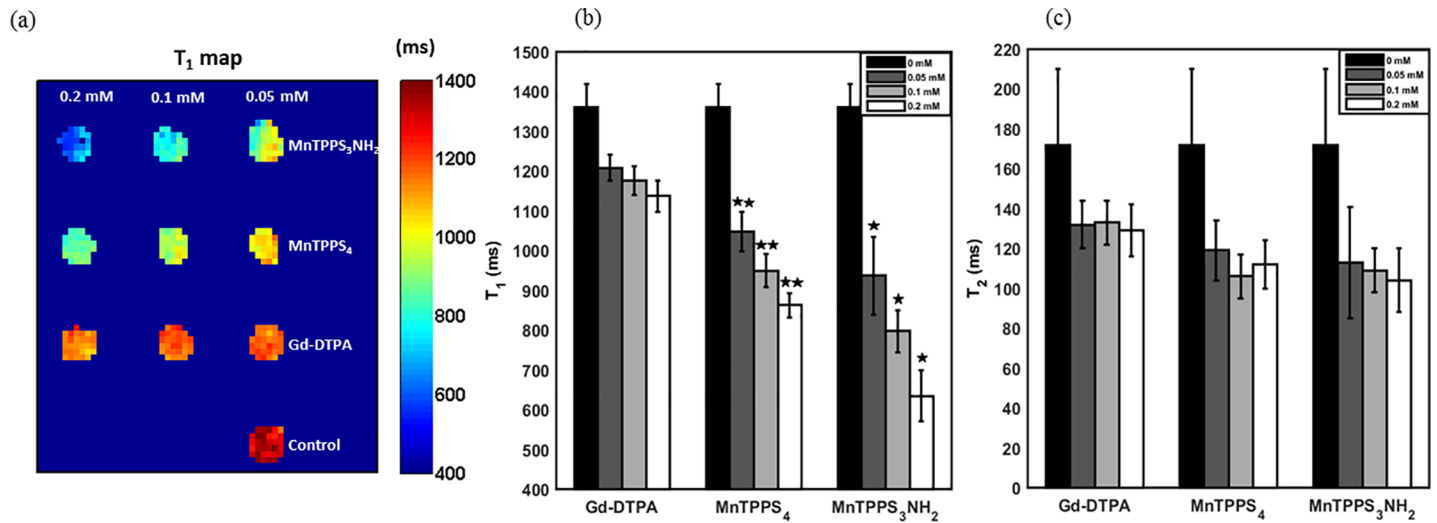


Fig 2. Quantitative MRI of CA direct exposure uptake in MDA-MB-231 cells. (a) A quantitative map of T_1 relaxation times of the CA direct exposure cell pellets. (b) T_1 and (c) T_2 relaxation times of the CA direct exposure cell pellets. Shown are mean values \pm standard deviation from all the pixels within each ROI in Fig 2A. *Indicates significant difference ($P < 0.05$) from MnTPPS₄. ** Indicates significant difference ($P < 0.05$) from Gd-DTPA.

<https://doi.org/10.1371/journal.pone.0196998.g002>

within each ROI in the quantitative map of T_1 relaxation times, Fig 3A. The largest decrease in the averaged T_1 time of the MnTPPS₃NH₂-labelled cell pellet at 0.2 mM (26.2%) corresponds to the greatest positive signal enhancement on T_1 -weighted MRI compared to the unlabelled cell pellet. MnTPPS₄ provided a 17.4% reduction in T_1 ($P < 0.05$), whereas Gd-DTPA enabled only a 7.1% decrease in T_1 ($P < 0.05$) at 0.2 mM, both relative to unlabelled cell pellet.

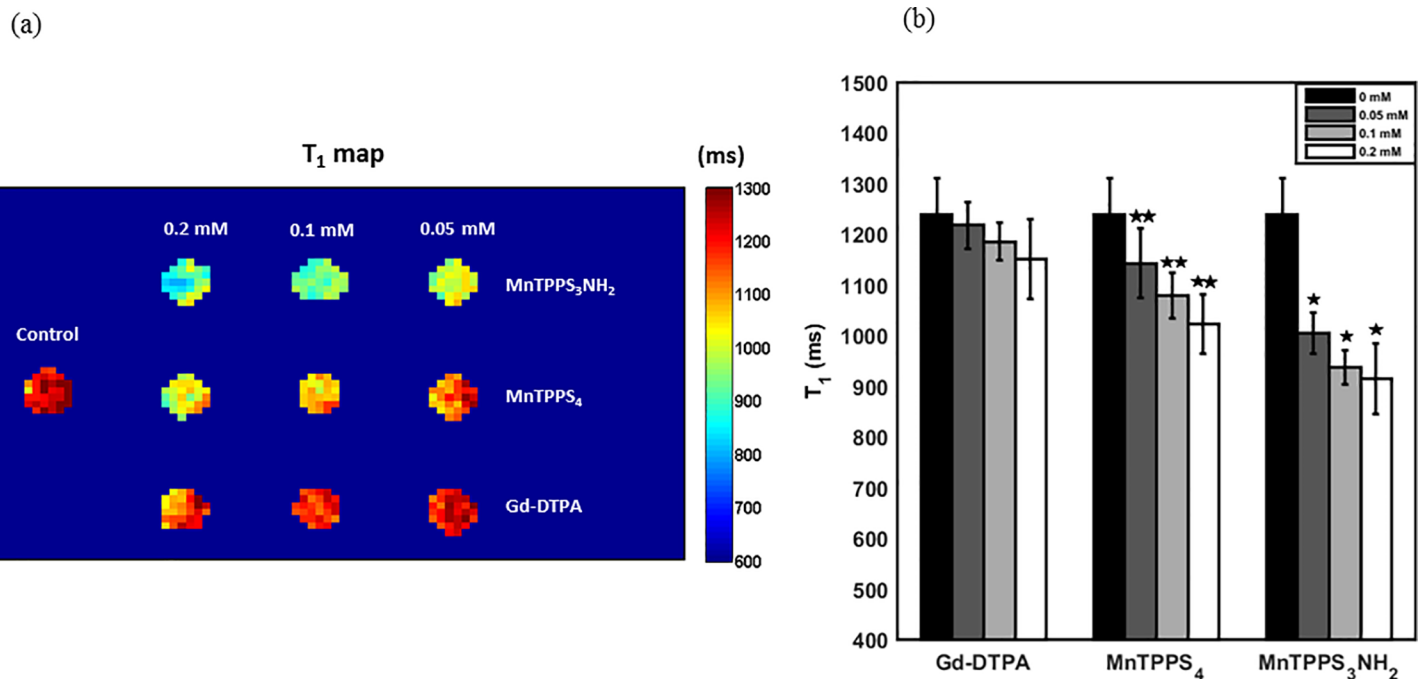


Fig 3. Quantitative MRI of CA retention in MDA-MB-231 cells. (a) A quantitative map of T_1 relaxation times of CA cellular retention pellets imaged 24–27 hrs post-cell labelling. (b) T_1 relaxation times of CA cellular retention pellets. Shown are mean values \pm standard deviation from all the pixels within each ROI in Fig 3A. *Indicates significant difference ($P < 0.05$) from MnTPPS₄. ** Indicates significant difference ($P < 0.05$) from Gd-DTPA.

<https://doi.org/10.1371/journal.pone.0196998.g003>

The difference among T_1 times of the three CAs is statistically significant at the examined concentrations (0.05–0.2 mM): MnTPPS₃NH₂ resulted in a 10.6% to 13.1% ($P < 0.05$) reduction in T_1 compared to MnTPPS₄, which enabled a further 6.1% to 11.1% ($P < 0.05$) decrease in T_1 compared to Gd-DTPA. At 0.05 mM, Gd-DTPA-induced decrease in T_1 from unlabelled control is statistically insignificant (95% confidence interval = [-8.8, 50.6] ms).

Graph of T_1 relaxation times of CA-labelled MDA-MB-231 cell pellets at 0 and 24–27 hrs post-cell labelling is shown in Fig 4 for the three CAs at the highest incubation concentration, 0.2 mM. The values represent mean \pm standard deviation from all the pixels within each one of the 6 respective ROIs in the quantitative maps of T_1 relaxation time in Figs 2A and 3A. Compared to Gd-DTPA, MnTPPS₃NH₂ enabled more than 44% and 20% ($P < 0.05$) reduction in T_1 immediately and 24–27 hrs post-cell labelling, respectively, whereas MnTPPS₄ resulted in more than 24% and 11% ($P < 0.05$) decrease in T_1 immediately and 24–27 hrs post-cell labelling, respectively, both at 0.2 mM.

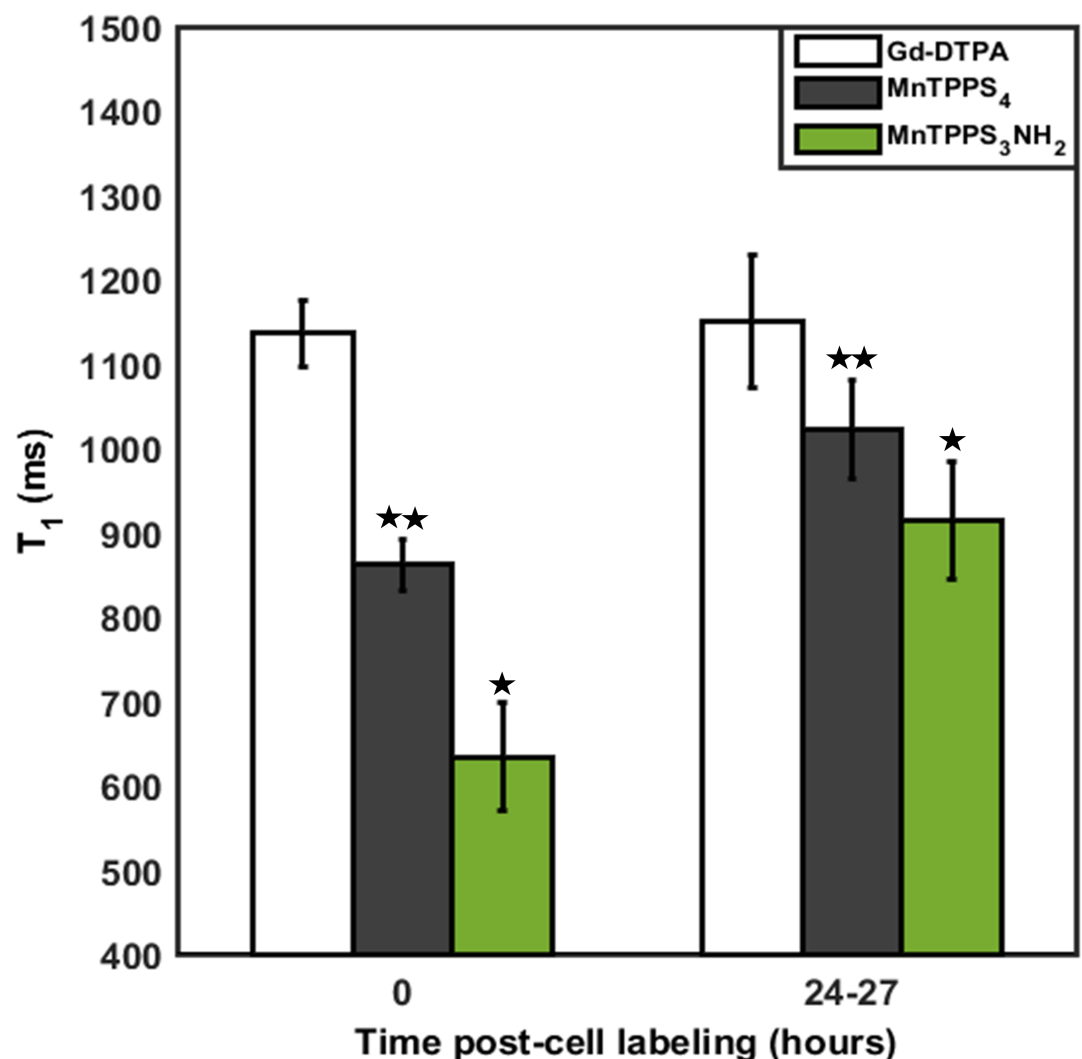


Fig 4. Comparison of CA direct exposure uptake and retention. Averaged T_1 relaxation times of CA-labelled MDA-MB-231 cell pellets at 0 and 24–27 hrs post-cell labelling for the three CAs at 0.2 mM. Shown are mean values \pm standard deviation from pixels within the respective ROIs in Figs 2A and 3A. * Indicates significant difference ($P < 0.05$) from MnTPPS₄. ** Indicates significant difference ($P < 0.05$) from Gd-DTPA.

<https://doi.org/10.1371/journal.pone.0196998.g004>

Cytotoxicity assessment of CA-labelled breast cell lines

The *in vitro* cytotoxicity assessment results from CA-labelled breast cell lines at 0.2 mM are summarized in Table 3. The values represent the averaged cellular viability, normalized relative to unlabelled cells, from 5 independent measurements ± standard deviation.

Quantitative MRI for sensitive detection of multiple clinical subtypes of breast cancer

Quantitative maps of T₁ relaxation times for MDA-MB-231, MCF-7, ZR-75-1, and MCF-10A cells are shown in Fig 5A–5D, along with pictures of cell pellets. Table 4 summarizes the T₁ times of the four breast cell lines. The values represent mean ± standard deviation from at least 30 measurements (pixels) within each ROI in the quantitative maps of T₁, Fig 5A–5D. Student’s t-test revealed that differences among the cell pellets’ T₁ times are statistically significant at 95% confidence level. More specifically, relative to Gd-DTPA, MnTPPS₃NH₂ enabled highly-sensitive detection of the four breast cell lines by depressing T₁ by 36.6% (MDA-MB-231), 43.1% (MCF-7), 35.6% (ZR-75-1), and 39.7% (MCF-10A), whereas MnTPPS₄ decreased T₁ by 26.0% (MDA-MB-231), 31.7% (MCF-7), 18.5% (ZR-75-1), and 14.3% (MCF-10A).

Discussion

Because a primary breast tumor mass can be associated with multiple subtypes, possessing diverse biologic profiles, histopathologies, and clinical outcomes [26], it is critical to enable quantitative imaging of various subtypes of breast cancer cells with sufficient sensitivities. Consequently, this work aimed at exploring, and potentially furthering, the oncological capabilities of MRI as a quantitative cellular modality by investigating the potential of MnP-enhanced MRI in detecting multiple clinical subtypes of breast cancer *in vitro*. This promising cellular imaging approach may overcome many limitations associated with conventional Gd-DTPA-enhanced MRI, including narrow post-contrast imaging window.

To compare the degree of positive contrast the examined T₁ CAs (MnTPPS₃NH₂, MnTPPS₄, and Gd-DTPA) can provide at 3.0T and to determine whether or not they suffer from any T₂-related negative signal effects, longitudinal and transverse relaxivities, r₁ and r₂, were calculated. MnTPPS₃NH₂ and MnTPPS₄ produced an over two-and-a-half-fold and two-fold increase in r₁, respectively, over Gd-DTPA. Similar fold change was previously reported for MnTPPS₄ and Gd-DTPA [12,15] and may be attributed, in part, to the anisotropy of the Mn³⁺ ground-state wavefunction in the porphyrin molecule which can bring the spin density of the manganese ions closer to the ¹H nuclei of the coordinated H₂O molecules [27]. However, the r₂/r₁ ratios for the three CAs are close to unity at relatively low CA concentrations, indicating that the effect of the CAs on T₁ relaxation times is considerably greater than that on T₂ due to the inherent longer T₁ times of biologic tissues.

Table 3. Cytotoxicity results of CA-labelled breast cell lines at 0.2 mM.

Cell line / CA	Gd-DTPA	MnTPPS ₄	MnTPPS ₃ NH ₂
MCF-10A	101.6 ± 5.5%	100.7 ± 3.1%	99.7 ± 4.7%
MCF-7	99.2 ± 6.8%	106.7 ± 10.9%	103.6 ± 5.1%
ZR-75-1	100.9 ± 4.6%	102.6 ± 1.0%	102.4 ± 3.3%
MDA-MB-231	99.5 ± 3.0%	104.1 ± 7.3%	99.4 ± 3.2%

CA: contrast agent. The values represent the mean normalized viability, relative to unlabelled cells, from 5 independent measurements ± standard deviation.

<https://doi.org/10.1371/journal.pone.0196998.t003>

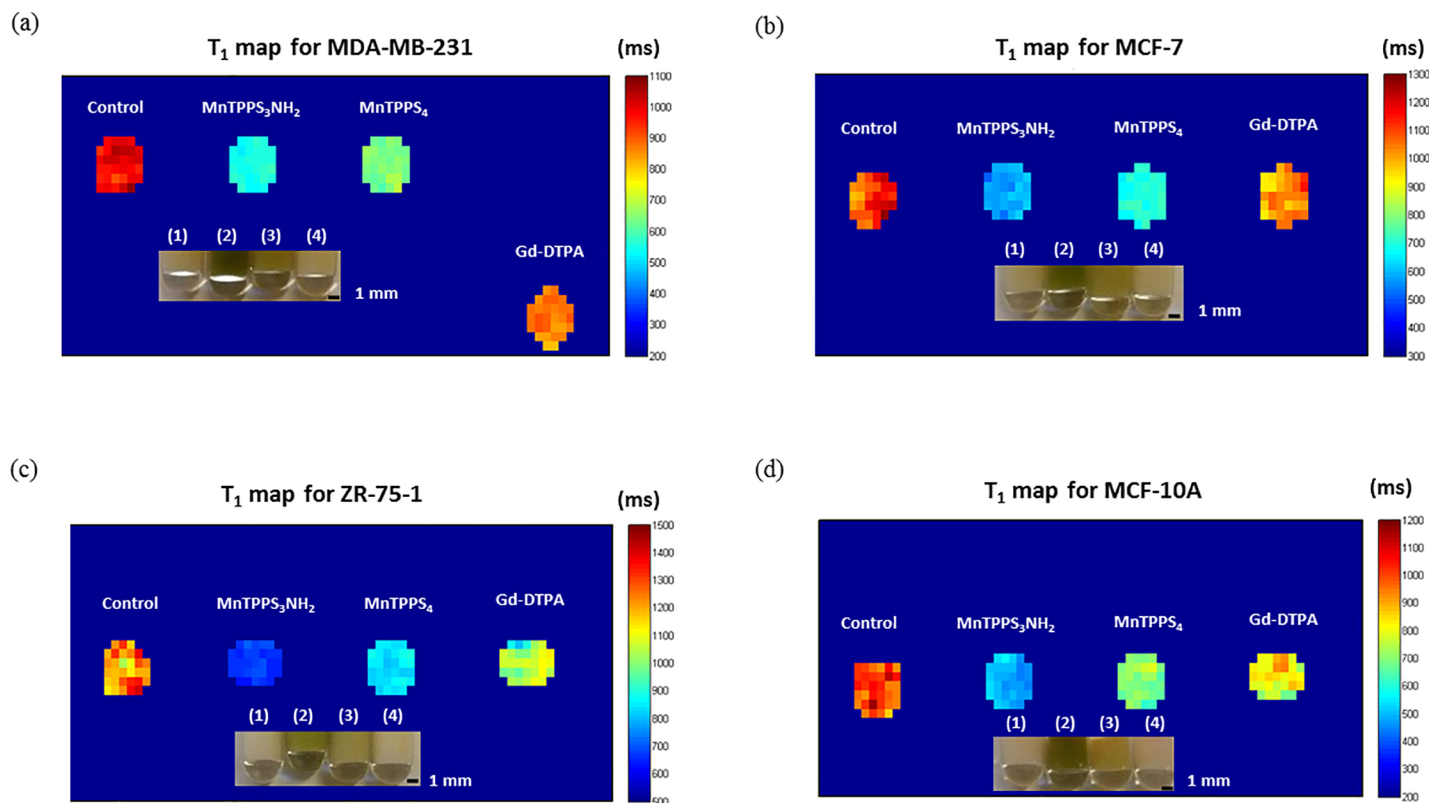


Fig 5. Quantitative maps of T_1 relaxation times of breast cell lines. (a) MDA-MB-231 (b) MCF-7 (c) ZR-75-1 and (d) MCF-10A cell pellets labelled with MnTPPS₃NH₂, MnTPPS₄, and Gd-DTPA at 0.2 mM. Shown also are pictures of the CA-labelled cell pellets: (1) Control; (2) MnTPPS₃NH₂; (3) MnTPPS₄; (4) Gd-DTPA.

<https://doi.org/10.1371/journal.pone.0196998.g005>

For the subsequent cell labelling studies, the reductions in T_1 relaxation times were taken as a direct measure of CA cellular uptake and the resulting MR signal enhancement. This assumption, which has also been applied by others [12,28], is likely to be valid because the relaxation rates in aqueous solution (Fig 1), in aggressive breast cancer cells (Fig 2B), and in tissue extracts [12,29] are proportional to CA concentrations. Moreover, a qualitative observation of the MnP-labelled cell pellets (S4 Fig) reveals a difference in the colour intensity of the pellets which is an evidence that higher cellular uptake of MnP (i.e. darker cell pellet color) translates to a greater T_1 reduction on MRI. Nevertheless, it should be noted that the relaxivities of CAs can generally be altered by binding to macromolecules [12], distribution of H₂O

Table 4. T_1 relaxation times (ms) for CA-labelled cells at 0.2 mM.

Cell line / CA	Control	MnTPPS ₃ NH ₂	MnTPPS ₄	Gd-DTPA
MDA-MB-231	992.8 ± 34.5	551.7 ± 15.5*	643.5 ± 20.5**	869.9 ± 26.1
MCF-7	1119.5 ± 77.6	583.8 ± 25.8*	700.0 ± 22.6**	1025.4 ± 54.0
ZR-75-1	1226.4 ± 84.7	667.7 ± 18.4*	845.2 ± 23.7**	1036.7 ± 70.7
MCF-10A	998.1 ± 61.4	489.5 ± 30.6*	695.9 ± 35.1**	812.2 ± 63.6

The values represent mean from at least 30 measurements ± standard deviation.

*Indicates significant difference ($P < 0.05$) from MnTPPS₄.

** Indicates significant difference ($P < 0.05$) from Gd-DTPA.

<https://doi.org/10.1371/journal.pone.0196998.t004>

protons [29], entrapment in subcellular compartments, and/or simply demetallization. Because the goal was to examine the MR signal enhancement characteristics of the T_1 CAs, however, the relative changes in the longitudinal relaxation times are the relevant measurements used in this investigation.

The MRI contrast enhancement patterns of the three CAs at 3.0T were investigated by labelling aggressive breast cancer cells, MDA-MB-231, with the CAs at various concentrations and incubation conditions (i.e. direct exposure and cellular retention). The statistically significant differences in T_1 times across the CA-labelled cell pellets attest to the dose-dependent T_1 response of the three CAs and suggest that, as mentioned earlier, the longitudinal relaxation rates of the cells are proportional to concentration of CAs and presumably cellular uptake. On the other hand, being T_1 CAs, their induced dose-dependent changes on T_2 times are primarily insignificant.

In both the direct exposure and cellular retention experiments, labelling cells with MnTPPS₃NH₂ at 0.2 mM yielded the most sensitive detection of MDA-MB-231 cells on T_1 -weighted MRI as it enabled a 53.3% and 26.2% decrease in T_1 from baseline, respectively. MnTPPS₄ also offered a sensitive detection by providing a 36.6% (direct exposure) and 17.4% (cellular retention) depression in T_1 from baseline, whereas Gd-DTPA only provided a 16.5% (direct exposure) and 7.1% (cellular retention) reduction in T_1 from baseline at 0.2 mM. Despite the slight cellular uptake and positive T_1 enhancement induced by Gd-DTPA, which has also been reported in previous cell labelling studies [20,21], it is evident from these fundamental investigations that the two MnPs have greater cellular uptake and retention capabilities. The mechanism of this uptake is unknown, although previous work with MnTPPS₄ suggested that this is not due to interaction with heme-binding protein [28]. However, the observed increase in T_1 times of all CAs 24–27 hrs post-cell labelling, which corresponds to a decrease in positive signal enhancement on T_1 -weighted MRI, indicates that MDA-MB-231 cells did not fully retain the CAs when incubated in CA-free media. Such an increase in longitudinal relaxation times has also been observed with MnCl₂-labelled MDA-MB-231 cells incubated in CA-free media in a previous study [6] and may be attributed, in part, to MRI signal dilutions owing to the aggressive cancer cell proliferation.

Subsequent experiments thoroughly assessed the cytotoxicity of the administered CAs and demonstrated that a 24–27 hr labelling of four breast cell lines (MDA-MB-231, MCF-7, ZR-75-1, and MCF-10A) with the three CAs at 0.2 mM had no cytotoxic effects. Therefore, to assess the differential signal-enhancing capabilities of the CAs, MRI was performed after labelling the aforementioned four breast cell lines with the three CAs for approximately 24 hrs at 0.2 mM (direct exposure) and revealed a consistently significant ($P < 0.05$) sensitivity for cellular detection using MnPs over Gd-DTPA. This is likely due to MnPs' higher cellular uptake and r_1 relaxivities at 3.0T. As expected from their chemical structures (S1 Fig), MnTPPS₃NH₂ and MnTPPS₄ exhibited different T_1 signal enhancement patterns. MnTPPS₃NH₂ offered significantly greater ($P < 0.05$) reductions in T_1 compared to MnTPPS₄ in the four breast cell lines possibly due to its amino (-NH₂) group which makes the agent more hydrophobic, thereby increasing its cellular uptake. This advantage is expected to enable MnTPPS₃NH₂ to achieve a positive contrast enhancement similar to MnTPPS₄ but at lower doses, which can reduce potential systemic toxicity *in vivo*. Moreover, because structural modification of MnTPPS₄ only occurs at the periphery of the phenyl rings (by replacing one SO₄ with NH₂), it causes almost no change on the inner metal binding site of porphyrin and should have little influence on the metal binding stability of MnTPPS₃NH₂.

While this work has demonstrated that the two MnPs can enable a substantial positive contrast enhancement of multiple subtypes of breast cancer cells compared to Gd-DTPA, it also revealed that the non-tumorigenic cell line, MCF-10A, exhibited a considerable CA uptake

and T_1 enhancement. The mechanism behind this high CA uptake in MCF-10A cells is unclear and requires future investigation of the subcellular localization of porphyrins in tumorigenic and non-tumorigenic cell lines. Moreover, to confirm that the high positive signal enhancement obtained indeed corresponds to cellular uptake of paramagnetic CAs, it is suggested that future cellular MRI studies will incorporate an analytical method of absolute intracellular element quantification (e.g. inductively coupled plasma mass spectrometry, ICP-MS). However, it should be noted that the co-authors have evidence from ICP in many of the previous MnP studies that higher MR signal correlates positively with Mn ion content on a per-cell basis. Because this observation has been very repeatable in our studies [6,30,31], we can confidently use the MR signal as an imaging correlate of ion content.

While future *in vivo* work would be helpful to elucidate the pharmacokinetics and tumor contrast enhancement efficiency of the contrast agents, the goal of the current work was to demonstrate the capability MnPs in detecting multiple clinical subtypes of breast cancer cells. *In vitro* experiments on cell lines provide a more controlled setting to examine cell line-specific uptake of contrast agents. *In vivo* validation in animal models is an important next step but would be inappropriate as a first platform for testing because the *in vivo* environment presents many other confounders, such as differences in take-rates, that can obscure the scientific question we are pursuing at hand.

It is important to note that often times when new compounds are being discovered, there can be a bias for one compound over another because one property of the compound provides a greater advantage. In the case of Gd versus Mn, the Gd has a higher efficiency because it has 7 unpaired electrons compared to Mn, which has 5 unpaired electrons. For this reason alone, Gd is the champion, despite the fact that it is toxic. Furthermore, it is easier to chelate Gd more stably than Mn, which is a neurotoxin in its ionic form. However, with the Mn-based contrast agents presented in this paper, the porphyrin ring provides a very high thermodynamic stability. With the recent recognition that Gd is toxic and has been associated with safety concerns in patients, there is a renewed interest in finding alternatives to Gd. MnPs present a viable alternative.

Conclusions

Current oncological applications of Gd-DTPA-enhanced MRI rely on bulk manifestations in tumor morphology, imaged within a relatively short window, rather than early, pre-angiogenic changes at the cellular level driving these manifestations. Using quantitative cellular MRI, this work has demonstrated the potential of MnPs for sensitive imaging of multiple clinical subtypes of breast cancer cells due to their high relaxivities and cellular uptake and retention compared to Gd-DTPA, despite the observed positive enhancement from a non-tumorigenic cell line. This study has also demonstrated, for the first time, the potential of the more hydrophobic MnP, MnTPPS₃NH₂, as a T_1 CA for sensitive detection of various breast cancer cells *in vitro* using quantitative cellular MRI.

Supporting information

S1 Fig. The chemical structures of (a) MnTPPS₄ and (b) MnTPPS₃NH₂.
(TIF)

S2 Fig. Schematic diagram for the arrangement of replicates in the cytotoxicity assessment of CA-labelled breast cell lines in a 96-well plate.
(TIF)

S3 Fig. The ultraviolet-visible spectra for (a) MnTPPS₄ and (b) MnTPPS₃NH₂. (TIF)

S4 Fig. Picture of MnTPP₃NH₂-labelled MDA-MB-231 cell pellets at (1) 0.2 mM, (2) 0.1 mM, and (3) 0.05 mM. (TIF)

Acknowledgments

Financial support for this work was provided to H-LMC by the Heart & Stroke Foundation of Canada (# 000223), the Natural Sciences and Engineering Research Council of Canada (NSERC, # 355795), and SickKids Foundation. M.A. was supported by NSERC Alexander Graham Bell Canada Graduate Scholarship–Doctoral (CGS–D3) and Ontario Graduate Scholarship,. Y.L. was supported by National Science Foundation of China (NSFC, # 51303155). The authors thank Professor Raymond Reilly for fruitful discussions.

Author Contributions

Conceptualization: Mosa Alhamami, Xiao-an Zhang, Hai-Ling Margaret Cheng.

Data curation: Mosa Alhamami, Hai-Ling Margaret Cheng.

Formal analysis: Mosa Alhamami, Xiao-an Zhang, Hai-Ling Margaret Cheng.

Funding acquisition: Mosa Alhamami, Xiao-an Zhang, Hai-Ling Margaret Cheng.

Investigation: Mosa Alhamami, Xiao-an Zhang, Hai-Ling Margaret Cheng.

Methodology: Mosa Alhamami, Weiran Cheng, Xiao-an Zhang, Hai-Ling Margaret Cheng.

Project administration: Mosa Alhamami, Hai-Ling Margaret Cheng.

Resources: Weiran Cheng, Yuanyuan Lyu, Xiao-an Zhang, Hai-Ling Margaret Cheng.

Software: Mosa Alhamami, Hai-Ling Margaret Cheng.

Supervision: Christine Allen, Xiao-an Zhang, Hai-Ling Margaret Cheng.

Validation: Mosa Alhamami, Hai-Ling Margaret Cheng.

Visualization: Mosa Alhamami, Hai-Ling Margaret Cheng.

Writing – original draft: Mosa Alhamami.

Writing – review & editing: Mosa Alhamami, Christine Allen, Hai-Ling Margaret Cheng.

References

1. Saslow D, Boetes C, Burke W, Harms S, Leach MO, Lehman CD, et al. American Cancer Society guidelines for breast screening with MRI as an adjunct to mammography. *CA Cancer J Clin.* 2007; 57: 75–89. <https://doi.org/10.1097/01.ogx.0000269073.50925.38> PMID: 17392385
2. Kuo PH, Kanal E, Abu-Alfa AK, Cowper SE. Gadolinium-based MR contrast agents and nephrogenic systemic fibrosis. *Radiology.* 2007; 242: 647–649. <https://doi.org/10.1148/radiol.2423061640> PMID: 17213364
3. Rohrer M, Bauer H, Mintorovitch J, Requardt M, Weinmann H-J. Comparison of magnetic properties of MRI contrast media solutions at different magnetic field strengths. *Invest Radiol.* 2005; 40: 715–724. <https://doi.org/10.1097/01.ri.0000184756.66360.d3> PMID: 16230904
4. Brant WE, Helms CA. *Fundamentals of diagnostic radiology.* Philadelphia, PA: Wolters Kluwer/Lippincott Williams & Wilkins; 2012.
5. Okuhata Y. Delivery of diagnostic agents for magnetic resonance imaging. *Adv Drug Deliv Rev.* 1999; 37: 121–137. [https://doi.org/10.1016/S0169-409X\(98\)00103-3](https://doi.org/10.1016/S0169-409X(98)00103-3) PMID: 10837731

6. Nofiele JT, Czarnota GJ, Cheng H-LM. Noninvasive manganese-enhanced magnetic resonance imaging for early detection of breast cancer metastatic potential. *Mol Imaging*. 2014; 13: 1–10. <https://doi.org/10.2310/7290.2013.00071> PMID: 24622809
7. Alhamami M, Mokhtari RB, Ganesh T, Nofiele JT, Yeger H, Cheng H-LM. Manganese-enhanced magnetic resonance imaging for early detection and characterization of breast cancers. *Mol Imaging*. 2014; 13: 1–8. <https://doi.org/10.2310/7290.2014.00021>
8. Ganesh T, Mokhtari RB, Alhamami M, Yeger H, Cheng H-LM. Manganese-enhanced MRI of minimally gadolinium-enhancing breast tumors. *J Magn Reson Imaging*. 2015; 41: 806–813. <https://doi.org/10.1002/jmri.24608> PMID: 24591227
9. Cheng W, Haedicke IE, Nofiele JT, Martinez F, Beera K, Scholl TJ, et al. Complementary strategies for developing Gd-free high-field T1 MRI contrast agents based on Mn Porphyrins. *J Med Chem*. 2014; 57: 516–520. <https://doi.org/10.1021/jm401124b> PMID: 24328058
10. Nofiele JT, Haedicke IE, Zhu YLK, Zhang X, Cheng H-LM. Gadolinium-free extracellular MR contrast agent for tumor imaging. *J Magn Reson Imaging*. 2015; 41: 397–403. <https://doi.org/10.1002/jmri.24561> PMID: 24399613
11. Mouraviev V, Venkatraman TN, Tovmasyan A, Kimura M, Tsivian M, Mouravieva V, et al. Mn porphyrins as novel molecular magnetic resonance imaging contrast agents. *J Endourol*. 2012; 26: 1420–1424. <https://doi.org/10.1089/end.2012.0171> PMID: 22783812
12. Furmanski P, Longley C. Metalloporphyrin enhancement of magnetic resonance imaging of human tumor xenografts in nude mice. *Cancer Res*. 1988; 48: 4604–4610. PMID: 3396012
13. Lyon RC, Faustino PJ, Cohen JS, Katz A, Mornex F, Colcher D, et al. Tissue distribution and stability of metalloporphyrin MRI contrast agents. *Magn Reson Med*. 1987; 4: 24–33. PMID: 3821476
14. Fiel RJ, Mark E, Button T, Gilani S, Musser D. Mechanism of the localization of manganese (III) meso-tetra(4-sulfonatophenyl)porphine in mice bearing L1210 tumors. *Cancer Lett*. 1988; 40: 23–32. PMID: 3370627
15. Cheng H-LM, Haedicke IE, Cheng W, Tchouala Nofiele J, Zhang X. Gadolinium-free T1 contrast agents for MRI: Tunable pharmacokinetics of a new class of manganese porphyrins. *J Magn Reson Imaging*. 2014; 40: 1474–80. <https://doi.org/10.1002/jmri.24483> PMID: 24214904
16. Alvares RDA, Szulc DA, Cheng H-LM. A scale to measure MRI contrast agent sensitivity. *Sci Rep*. Springer US; 2017; 7: 15493. <https://doi.org/10.1038/s41598-017-15732-8> PMID: 29138455
17. Place DA, Faustino PJ, van Zijl PCM, Chesnick A, Cohen JS. Metalloporphyrins as contrast agents for tumors in magnetic resonance imaging. *Invest Radiol*. 1990; 25: S69–S70. PMID: 2283262
18. Place DA, Faustino PJ, Berghmans KK, van Zijl PCM, Chesnick AS, Cohen JS. MRI contrast-dose relationship of manganese (III) tetra (4-sulfonatophenyl) porphyrin with human xenograft tumors in nude mice at 2.0 T. *Magn Reson Imaging*. 1992; 10: 919–928. PMID: 1461089
19. Bockhorst K, Hohn-Berlage M, Kocher M, Hossmann K-A. Proton relaxation enhancement in experimental brain tumors—in vivo NMR study of manganese(III)TPPS in rat brain gliomas. *Magn Reson Imaging*. 1990; 8: 499–504. PMID: 2392036
20. Digilio G, Menchise V, Gianolio E, Catanzaro V, Carrera C, Napolitano R, et al. Exofacial protein thiols as a route for the internalization of Gd(III)-based complexes for magnetic resonance imaging cell labeling. *J Med Chem*. 2010; 53: 4877–4890. <https://doi.org/10.1021/jm901876r> PMID: 20533827
21. Giesel FL, Stroick M, Griebe M, Troster H, von der Lieth CW, Requardt M, et al. Gadofluorine M uptake in stem cells as a new magnetic resonance imaging tracking method: An in vitro and in vivo study. *Invest Radiol*. 2006; 41: 868–873. <https://doi.org/10.1097/01.rli.0000246147.44835.4c> PMID: 17099425
22. Shuai H, Shi C, Lan J, Chen D, Luo X. Double labelling of human umbilical cord mesenchymal stem cells with Gd-DTPA and PKH26 and the influence on biological characteristics of hUCMSCs. *Int J Exp Pathol*. 2015; 96: 63–72. <https://doi.org/10.1111/iep.12111> PMID: 25649907
23. Zhang Z, He R, Yan K, Guo Q ni, Lu Y guo, Wang X xia, et al. Synthesis and in vitro and in vivo evaluation of manganese(III) porphyrin-dextran as a novel MRI contrast agent. *Bioorganic Med Chem Lett*. Elsevier Ltd; 2009; 19: 6675–6678. <https://doi.org/10.1016/j.bmcl.2009.10.003> PMID: 19850475
24. Holliday DL, Speirs V. Choosing the right cell line for breast cancer research. *Breast Cancer Res*. 2011; 13: 215. <https://doi.org/10.1186/bcr2889> PMID: 21884641
25. Subik K, Lee J-F, Baxter L, Strzepak T, Costello D, Crowley P, et al. The Expression Patterns of ER, PR, HER2, CK5 /6, EGFR, Ki-67 and AR by Immunohistochemical Analysis in Breast Cancer Cell Lines. *Breast Cancer Basic Clin Res*. 2010; 4: 35–41.
26. Vargo-Gogola T, Rosen JM. Modelling breast cancer: one size does not fit all. *Nat Rev Cancer*. 2007; 7: 659–672. <https://doi.org/10.1038/nrc2193> PMID: 17721431
27. Koenig SH, Brown RD, Spiller M. The anomalous relaxivity of Mn³⁺(TPPS₄). *Magn Reson Med*. 1987; 4: 252–260. PMID: 3574059

28. Megnin F, Faustino PJ, Lyon RC, Lelkes PI, Cohen JS. Studies on the mechanism of selective retention of porphyrins and metalloporphyrins by cancer cells. *Biochim Biophys Acta*. 1987; 929: 173–181. PMID: [3593779](#)
29. Braunschweiger PG, Schiffer LM, Furmanski P. ¹H-NMR relaxation times and water compartmentalization in experimental tumor models. *Magn Reson Imaging*. 1986; 4: 335–342. PMID: [3669948](#)
30. Haedicke IE, Li T, Zhu YLK, Martinez F, Hamilton AM, Murrell DH, et al. An enzyme-activatable and cell-permeable Mn^{III}-porphyrin as a highly efficient T₁ MRI contrast agent for cell labeling. *Chem Sci*. 2016; 7: 4308–4317. <https://doi.org/10.1039/C5SC04252F>
31. Loai S, Haedicke I, Mirzaei Z, Simmons CA, Zhang X-A, Cheng HL. Positive-contrast cellular MRI of embryonic stem cells for tissue regeneration using a highly efficient T₁ MRI contrast agent. *J Magn Reson Imaging*. 2016; 44: 1456–1463. <https://doi.org/10.1002/jmri.25299> PMID: [27185221](#)